Food Chemistry: X 24 (2024) 101835

Contents lists available at ScienceDirect

Food Chemistry: X

journal homepage: www.sciencedirect.com/journal/food-chemistry-x

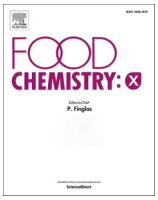

An aptasensor with colorimetric and electrochemical dual-outputs for malathion detection utilizing peroxidase-like activity of Fe-MOF

Xu Yiwei [a,*], Jia Xupeng [a], Yang Sennan [b], Cao Mengrui [a], He Baoshan [a,*], Ren Wenjie [a], Suo Zhiguang [a]

[a] National Engineering Laboratory/Key Laboratory of Henan province, School of Food Science and Technology, Henan University of Technology, Zhengzhou 450001, China
[b] Henan Institute of Food and Salt Industry Inspection Technology, Zhengzhou 450003, China

ARTICLE INFO

Keywords:
Aptasensor
Colorimetric
Electrochemical
Malathion
Nanoenzyme

ABSTRACT

An aptasensor with dual-outputs was developed for malathion detection. Fe-MOF was synthesized to design favorable signal probes for catalytic amplification. Owing to the excellent peroxidase-like activity of Fe-MOF, the redox reaction was catalyzed to produce the dual-outputs of colorimetric and electrochemical. In this sensing strategy, malathion was captured by the aptamer on sensing interface, leading to the release of signal probe. Thanks to the catalytic amplification of Fe-MOF and the high capture effect of aptamer, the aptasensor produced a sensitive response for malathion. Based on the dual-signals of absorbance and current, the detection method for malathion was developed ranging from 10 ng/mL to 500 ng/mL. The detection limit of malathion was 5.8 ng/mL for colorimetric output and 4.6 ng/mL for electrochemical output. Furthermore, the aptasensor exhibited high specificity and good repeatability in malathion detection. Finally, the aptasensor was applied to detect malathion in fruit and vegetable samples with satisfactory recovery.

1. Introduction

Pesticides play an important role to eradicate pests, control vectors of the diseases, and improve productivity for agriculture. However, their residues can remain in plant tissues, and cause problems to human health. There are about three million cases of pesticides poisoning every year, where the most common pesticides are organophosphates (Abdo et al., 2021). Organophosphorus pesticides are a type of organic chemicals containing phosphorus. Organophosphorus pesticides are annually used up to 2 million tons worldwide, and it is approximately 40 % of total global pesticide usage (W. Li et al., 2023). Malathion is one of the most commonly used organophosphate pesticides in planting of fruit and vegetable. It is also commonly used as a protectant in storage of agricultural products. The primary toxicity mechanism of malathion is the inhibition of the activity of cholinesterase and subsequent accumulation of the neurotransmitter acetylcholine. Human body exposed to malathion may be related to a variety of clinical conditions, including cancer, reproductive problems and neurological disorders (Pupim et al., 2023). The quantitative determination of malathion is necessary for health. Traditionally, malathion was detected by precise instrument, including high-performance liquid chromatography (Bazmandegan-Shamili, Haji Shabani, Dadfarnia, Rohani Moghadam, & Saeidi, 2017), gas chromatography and mass spectrometry (Gupta, Singh, Nayak, Das, & Jan, 2022). Reliable detection results can be obtained by these methods. Nonetheless, they suffer from some drawbacks, such as time-consuming and labor-intensive analysis procedure. Therefore, it still needs to explore sensitive and selective method for malathion detection.

Sensing techniques possess significant advantages of high efficiency, fast response and convenient operation in quantitative analysis (Liang et al., 2021). Recently, a series of sensing methods have been developed for malathion measurement, such as colorimetric (P. Li, Zhan, Tao, Xie, & Huang, 2023), electrochemical (C. Zhu, Wang, Yu, Chen, & Han, 2023), fluorescence (Chen et al., 2020), and surface-enhanced Raman spectroscopy (Serebrennikova, Komova, Aybush, Zherdev, & Dzantiev, 2023). Among these methods, colorimetric and electrochemical attract much attention. Colorimetric method is convenient to rapidly achieve the target information by the visual color change. Generally, the triggered color change can be directly observed by the naked eye, and it is easy to obtain the measurable color signal by spectrometer or camera (Thajee, Paengnakorn, Wongwilai, & Grudpan, 2018). Electrochemical

* Corresponding authors.
E-mail addresses: xu_yiwei@126.com (X. Yiwei), baoshanhe2008@haut.edu.cn (H. Baoshan).

https://doi.org/10.1016/j.fochx.2024.101835
Received 12 July 2024; Received in revised form 11 September 2024; Accepted 11 September 2024
Available online 17 September 2024

is another reliable analysis method. In comparison with optical methods, the electrochemical signal is produced by the electron transfer reaction on working electrode, which is not susceptible to external environmental factors of light, temperature and humidity. In order to achieve advantages of both methods, it is required to develop a sensor with the dual-outputs of colorimetric and electrochemical. Besides, the detection result from dual-signals method is more reliable than that of single-signal method, because the outcomes obtained from dual-signals method can be used to verify each other.

In order to improve the sensitivity of sensors, enzymes are usually employed as catalytic labels for signal amplification. For example, peroxidase is often used to catalyze H_2O_2-mediated redox reaction in colorimetric and electrochemical analysis. The substrate can be oxidized by peroxidase, and then produces color or current change. Peroxidase usually plays an important role in colorimetric and electrochemical sensors. However, natural enzymes have intrinsic disadvantages such as high production cost, low operational stability, difficult preparation, and susceptibility to denaturation. To overcome these drawbacks of natural enzyme, nanomaterials have been explored to imitate the catalytic activity of enzyme, which are known as nanoenzymes (Li et al., 2023). Compared with natural enzymes, nanoenzymes have unique features, including low cost, high stability and easy preparation (Shu et al., 2022). Inspired by the catalysis of Fenton's reagent (containing Fe^{2+}/Fe^{3+} ions), the nanomaterial with intrinsic peroxidase-like activity is firstly discovered in Fe_3O_4 nanoparticles (Gao et al., 2007). After that, lots of nanomaterials have been proved with the peroxidase-like catalytic activity (Wang, Dong, & Wei, 2023). Metal-organic frameworks (MOFs) are a kind of crystalline porous materials formed by self-assembly of inorganic metals and organic ligands via coordination bonds. Because metal nodes and organic ligands of MOFs are similar to the reaction centers of natural enzymes, MOFs are found with excellent enzyme-like activity (Zhang et al., 2019). Therefore, MOFs have a great prospect in the preparation of sensors with colorimetric and electrochemical dual-outputs.

The interference of complex matrices in real samples still poses a challenge to precisely quantify malathion. To eliminate the interference, it is required for sensing interface to recognize malathion specifically. Aptamer, as a single-stranded and short oligonucleotide molecule, has high affinity and specificity for the target. In contact with the target, aptamer can form a complex three-dimensional structure to bind with the target (Davydova & Vorobyeva, 2024). In comparison with antibodies, aptamers offer distinct advantages such as simple synthesis, long-term stability and site-directed label. Since the malathion specific aptamer has been selected by a systematic evolution of ligands by exponential enrichment process (Williams, Maher, & Sooter, 2014), it has been applied to prepare various of single-signal aptasensors, including surface-enhanced Raman scattering (Nie et al., 2018), colorimetric (Bala, Mittal, Sharma, & Wangoo, 2018), fluorescence (Bala et al., 2018), and electrochemical sensors (Xu et al., 2021). Therefore, the aptamer is an ideal recognition element for the fabrication of malathion sensor with dual-outputs.

In this work, an aptasensor with colorimetric and electrochemical dual-outputs was proposed for malathion detection utilizing aptamer as recognition element and Fe-MOF as signal producer. The malathion-binding aptamer was immobilized on a microplate (MP) by the biotin-streptavidin interaction. The Fe-MOF was synthesized by a solvothermal method, and then bonded with the complementary DNA (cDNA) of aptamer utilizing Au nanoparticles (AuNPs) as linker. Based on the hybridization reaction between aptamer and cDNA molecules, Fe-MOF was attached to the microporous plate. Because of the peroxidase-like activity, Fe-MOF could catalyze 3, 3′, 5, 5′-tetramethyl benzidine (TMB) oxidation in presence of H_2O_2, producing measurable colorimetric and electrochemical signals. The sensing assay was developed on the specific capture of malathion by aptamer, resulting in the release of Fe-MOF from microporous plate. Benefiting from the specific recognition of aptamer and the catalytic amplification of Fe-MOF, the proposed dual-outputs aptasensor exhibited high sensitivity and selectivity.

2. Materials and methods

2.1. Reagents and materials

Acetic acid, sodium acetate, sodium citrate, TMB, trichloroethyl phosphate (TCEP), bovine serum albumin (BSA), chlorpyrifos, methyl-parathion, demeton, phoxim, malathion, pluronic F127, and phosphate buffered saline with 0.05 % (*v*/v) Tween-20 (PBST, pH = 8.0) were obtained from Shanghai Macklin Biochemical. $FeCl_3{\cdot}6H_2O$, $HAuCl_4{\cdot}3H_2O$, H_2O_2 (30 %), 2-aminoterephthalic acid (NH_2-BDC) and 3-aminophenol were purchased from Aladdin Reagent Co., Ltd. All chemical reagents were of analytical grade and used without further purification.

The sequence of malathion aptamer was selected according to previous study (Williams et al., 2014). The malathion aptamer was the following sequences: 5′-biotin-$(CH_2)_6$-ATC CGT CAC ACC TGC TCT TAT ACA CAA TTG TTT TTC TCT TAA CTT CTT GAC TGC TGG TGT TGG CTC CCG TAT-3′. The cDNA was the following sequences: 5′-(SH)-$(CH_2)_6$-ATA CGG GAG CCA ACA CCA-3′. They were synthesized by Shanghai Bioengineering Co., ltd.

2.2. Apparatus

The morphology was characterized using a JEM-F200 transmission electron microscope (JEOL, Japan). The Fourier transform infrared spectroscopy (FTIR) information was acquired using a Nicolet iS20 FTIR instrument (Thermo Scientific, America). The X-ray photoelectron spectroscopy (XPS) data were collected on an ESCALAB Xi+ XPS system (Thermo Scientific, America). The absorbance spectra were obtained using an AQ7100 spectrophotometer (Thermo Scientific, America). The amperometric i-t curve was acquired by a CHI 660E electrochemical workstation (Shanghai CH Instruments, China) with a screen-printed electrode: conductive carbon powder with 3 mm in diameter as working electrode, conductive carbon powder as counter electrode, Ag/AgCl as reference electrode (Changsha Sinjeen Electronic Technology, China). Malathion in fruit and vegetable samples was analyzed by an Agilent 7890B gas chromatography equipped with flame ionization detector (Agilent, America).

2.3. Synthesis of Fe-MOF/AuNPs/cDNA signal probe

Fe-MOF was synthesized by a hydrothermal method (Zhan et al., 2020). $FeCl_3{\cdot}6H_2O$ was served as the metal source. NH_2-BDC was employed as the organic linker. F127 surfactant and acetic acid were used as growth control agents. Firstly, 0.716 g of $FeCl_3{\cdot}6H_2O$ and 0.64 g of F127 were dissolved in 56 mL deionized water, and then stirred for 1 h. Secondly, 1.2 mL of acetic acid was added and stirred for 1 h. Thirdly, 0.24 g of NH_2-BDC was added and stirred for 2 h. The mixture obtained from the above steps was transferred to a Teflon-lined stainless-steel reactor for 24 h at 110 °C. Following that, the precipitate of Fe-MOF was collected by centrifugation at 8000 rpm for 5 min, and then washed with ethanol and deionized water for three times in turn. Finally, the prepared Fe-MOF was dried in a vacuum oven at 70 °C for further use.

Colloidal AuNPs were synthesized by a typical citrate reduction method (Y. Chen, Meng, Gu, Yi, & Sun, 2019). 4 mL trisodium citrate solution (1 %) was added to 100 mL boiling $HAuCl_4$ solution (0.01 %) under reflux for 10 min. It was observed that the solution color changed from yellow to wine-red, indicating the formation of AuNPs. The AuNPs solution was cooled to room temperature under continuous stirring, and stored at 4 °C. Fe-MOF/AuNPs was prepared by the addition of 100 mg of Fe-MOF to 30 mL of AuNPs solution under stirring, and followed by oscillation for 48 h. The obtained Fe-MOF/AuNPs was cleaned with ethanol and deionized water, and dispersed in 30 mL of 0.01 mol/L Tris-HCl (pH = 7.4) for later use.

The immobilization of cDNA on Fe-MOF/AuNPs was based on self-assembly. Firstly, 100 μL of TCEP solution (10 mmol/L) was added to 100 μL of cDNA stock solution (0.1 mmol/L) and reacted for 60 min to reduce disulfide bond. Subsequently, 100 mL of Fe-MOF/AuNPs dispersion was added to the above cDNA solution and incubated on a shaker for 12 h at 4 °C. In this process, cDNA was immobilized on Fe-MOF/AuNPs by S—Au bond. After incubation, the excess aptamer was removed by centrifugation. After that, the signal probe of Fe-MOF/AuNPs/cDNA was blocked by 1 % BSA. Finally, Fe-MOF/AuNPs/cDNA nanoparticles were rinsed and dispersed in 10 mL 0.01 mmol/L Tris-HCl (pH = 7.4) and stored at 4 °C for further use.

2.4. Preparation of Fe-MOF/AuNPs/cDNA/apt/MP aptasensor

The aptasensor of Fe-MOF/AuNPs/cDNA/Apt/MP was prepared by the following steps. Firstly, 100 μL of streptavidin solution (5 mg/mL) was added to a MP and incubated at 37 °C for 2 h. Subsequently, 100 μL of 1 % BSA solution was added to the plate and incubated at 37 °C for 2 h. The non-specific active sites on the plate surface were blocked by BSA. After that, 50 μL of 0.5 μmol/L biotin-labeled aptamer was added to the plate and incubated at 37 °C for 1 h. The Apt molecules were immobilized on plate surface via the streptavidin-biotin interaction to form Apt/MP. Finally, 50 μL of the Fe-MOF/AuNPs/cDNA dispersion was added to the plate and incubated at 37 °C for 1 h. The Fe-MOF/AuNPs/cDNA signal probe was combined with Apt/MP by complementary base pairing between Apt and cDNA. After each step, PBST (pH = 8.0) solution containing 0.05 % (*v*/v) Tween-20 was used to clean the plate. The aptasensor of Fe-MOF/AuNPs/cDNA/Apt/MP was formed by the above process.

2.5. Malathion detection

Malathion was detected by the following steps. Firstly, 50 μL malathion in Tris-HCl buffer solution (pH = 7.4) with different concentrations was added to Fe-MOF/AuNPs/cDNA/Apt/MP and incubated at 37 °C for 40 min. The malathion molecule bond to the aptamer, resulting in the release of Fe-MOF/AuNPs/cDNA signal probe. Subsequently, the MP was cleaned three times by PBST to remove the released signal probe. After that, 20 μL of 30 mmol/L TMB, 10 μL of 100 mmol/L H_2O_2 and 170 μL acetic acid buffer solution (0.2 mol/L, pH = 4) were added to the plate. After reaction for 10 min, the product signals of color and current were collected by UV–Vis spectrophotometer and electrochemical workstation.

2.6. Real sample analysis

Fruit and vegetable samples including apple, cabbage, carrot, celery, cowpea, eggplant, green pepper, pear, spinach and tomato, were purchased from a local supermarket (Zhengzhou, China). The wet weight of each kind of sample was at least 2 kg. Each kind of sample was minced by a food processer and mixed thoroughly. The sample size was 1 for each kind of sample. Approximately 10 g of sample was weighed and transferred into a 100 mL beaker. Then, 20 mL acetonitrile was added to this beaker. The mixture was homogenized by a homogenizer at 15000 r/min for 2 min. The filter liquor was transferred to a conical flask containing 3 g NaCl, and violently oscillated for 2 min. After 30 min of standing, 10 mL of supernatant was transferred to a centrifuge tube. This supernatant was evaporated to dryness at 80 °C under N_2. 200 μL of acetone was added to the test tube to dissolve the residue. After that, the extract was diluted to 5.0 mL with Tris-HCl buffer solution (10 mmol/L, pH = 7.4). Finally, the extract was filtered by a 0.22 μm filtration membrane for colorimetric and electrochemical analysis. For gas chromatography analysis, samples were pretreated in a similar way. The extract was diluted with acetone instead of Tris-HCl buffer solution. The recovery was evaluated by addition of malathion standard substance into these samples.

3. Results and discussion

3.1. Mechanism for malathion detection

The mechanism of aptasensor preparation and malathion detection was depicted in Fig. 1. The streptavidin modified MP was employed as the sensing platform for aptamer immobilization via the streptavidin-biotin interaction. In the preparation of signal probe, Fe-MOF was synthesized by a hydrothermal method and then coupled with cDNA utilizing AuNPs as the linker. After the hybridization between Apt and cDNA, the signal probe of Fe-MOF/AuNPs/cDNA anchored on Apt/MP to form the aptasensor of Fe-MOF/AuNPs/cDNA/Apt/MP. Owing to the peroxidase-like activity of Fe-MOF, the substrate of TMB was oxidized to oxTMB in presence of H_2O_2. Because oxTMB had a different color from TMB and was electroactive. The dual-outputs of colorimetric and electrochemical could be obtained by the prepared aptasensor. In presence of malathion, it competed with cDNA to combine with Apt, leading to the release of signal probe. The obtained signals were reduced in compared with its initial state. Therefore, malathion could be measured according to the signals change.

3.2. Characterization of the synthesized materials

The morphology of the synthesized Fe-MOF/AuNPs was surveyed by transmission electron microscope (TEM). From TEM images (Fig. 2a), Fe-MOF presented a spindle shape with uniform size. The length was about 1.2 mm, and the width was about 400 nm. It was observed that AuNPs as spots covered on the Fe-MOF surface. From EDS mapping images (Fig. 2b), it shown the distribution of C, N, O, Fe and Au elements in Fe-MOF/AuNPs. The FTIR spectrogram of Fe-MOF and the ligand NH_2-BDC was shown in Fig. 2c. The distinct peaks at 3506 cm^{-1} and 3392 cm^{-1} in HN_2-BDC were derived from the symmetric and asymmetric stretching vibration of N—H bond. These two peaks shifted to 3476 cm^{-1} and 3375 cm^{-1} in FTIR spectrum of Fe-MOF. It was ascribed to the formation of intra-framework hydrogen bonding of -NH_2 with an electron donating oxygen from -COOH (Yiwei et al., 2021). The wavenumber region of 2500–3300 cm^{-1} was derived from the O—H wagging vibrations of -COOH. Compared with HN_2-BDC, the transmittance in this wavenumber region was diminished in the spectra of Fe-MOF. It indicated that HN_2-BDC was deprotonated in the frameworks of Fe-MOF. The electronic structure of Fe-MOF was studied by XPS. From XPS spectrum (Fig. 2d-h), it depicted the binding energy of C 1 s at 284.5 eV and 288.2 eV, N 1 s at 398.8 eV, O 1 s at 531.4 eV, Fe 2p at 711.1 eV, 717.1 eV and 724.5 eV, respectively. There are two peaks at 285.0 eV and 288.3 eV in C 1 s spectrum corresponding to C—C and C—N bonds separately (Xie et al., 2020). The Fe 2p spectrum also included two peaks at 711.1 eV and 724.5 eV corresponding to Fe $2p_{3/2}$ and Fe$2p_{1/2}$ separately. A satellite signal was observed at 717.1 eV, suggesting the existence of Fe^{3+} in Fe-MOF (Li et al., 2018). The above results revealed the successful synthesis of Fe-MOF and Fe-MOF/AuNPs materials.

3.3. Peroxidase-like activity of Fe-MOF

In order to verify the peroxidase-like activity of Fe-MOF, the enzymatic kinetics curves were developed utilizing the substrates of TMB and H_2O_2. As shown in Fig. 3, with the increase of substrate concentration, the reaction speed increased initially and then gradually levelled off, which was consistent with the Michaelis-Menten model. The double reciprocal curve of substrate concentration and reaction rate showed a good linear relationship. The steady-state kinetic parameters of K_m and V_{max} were calculated according to the Lineweaver-Burk double reciprocal graph. When H_2O_2 was used as the substrate, K_m = 2.16 mM and $V_{max} = 1.98 \times 10^{-7}$ $M^{-1}s$. When TMB was used as the substrate, K_m = 0.66 mM, $V_{max} = 1.77 \times 10^{-7}$ $M^{-1}s$. Compared with other nanoenzymes (W.-C. Hu, Younis, Zhou, Wang, & Xia, 2020; Warkhade et al., 2021; Yılmaz, Ünlüer, Ersöz, & Say, 2018), the synthesized Fe-

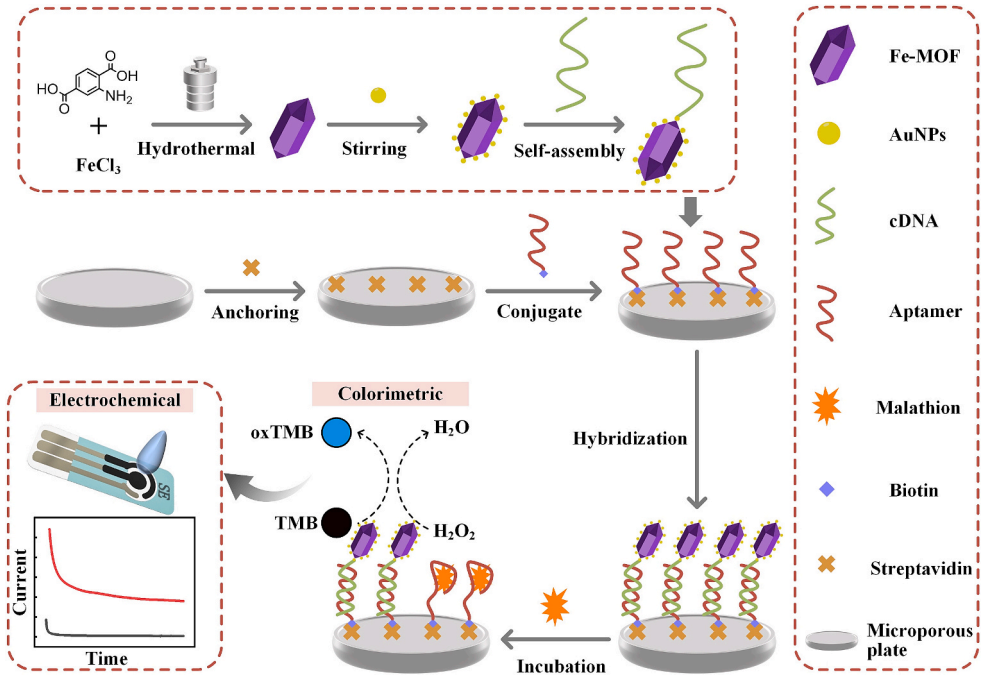

Fig. 1. Mechanism of aptasensor preparation and malathion detection.

MOF exhibited high V_{max} and low K_m value. High Vmax revealed a good catalytic effect, and low K_m suggested a strong affinity with the substrate. The above results indicated that the synthesized Fe-MOF has excellent peroxidase-like activity.

3.4. Optimization of aptasensor performance

To achieve the optimal performance of the aptasensor, key conditions were studied, including streptavidin concentration, Apt concentration, the hybridization time between Apt and cDNA, and the catalytic reaction time. These conditions were determined by the aptasensor outputs of absorbance value. From Fig. 4a, the absorbance value increased with the streptavidin concentration, and reached maximum at 5 μg/mL streptavidin. It was probably because the adsorbed streptavidin has reached saturation on the plate surface. From Fig. 4b, the absorbance value increased with the Apt concentration and levelled off at higher Apt concentration of 0.5 μmol/L. It was deduced that the density of Apt molecules on the plate surface almost reached maximum. From Fig. 4c, the absorbance value increased with the hybridization time and levelled off after 60 min, probably because the anchoring sits on the plate were almost completely occupied by hybridization between Apt and cDNA. From Fig. 4d, the absorbance value decreased with the incubation time for malathion and levelled off after 40 min. It could be attributed that the reaction has reached equilibration. These optimal conditions were used for subsequent study.

3.5. Analytical performance of the aptasensor

The prepared aptasensor with colorimetric and electrochemical dual-outputs was employed for detection of malathion. From Fig. 5a-d, the obtained dual-signals of absorbance and current decreased with the increased malathion concentration. Because malathion combined with Apt molecule, leading to the release of Fe-MOF from the aptasensor. Fe-MOF as a key catalyst, played an important role in the redox reaction. Therefore, the redox reaction was blocked in presence of malathion, resulting in the reduced signals of absorbance and current. The $\triangle$A and $\triangle$I were linearly depended on the logarithm of malathion concentration in the range from 10 ng/mL to 500 ng/mL. For absorbance signal, the linear regression was estimated as $\triangle A = 0.1672\log C - 0.1328$ ($R^2 = 0.9921$). For current signal, the linear regression was estimated to be $\triangle I = 1.2215\log C - 0.7184$ ($R^2 = 0.9969$). Based on the signal-to-noise ratio of 3, the limit of detection (LOD) was calculated to be 5.8 ng/mL for absorbance signal and 4.6 ng/mL for current signal. Compared with other sensors (Faghiri, Hajjami, & Ghorbani, 2021; Liu et al., 2021; Rizk et al., 2023), the prepared aptasensor exhibited low LOD and high sensitivity for malathion detection. These advantages derived from the synergistic effect of Apt and Fe-MOF: the Apt molecule had a high affinity for malathion, and the synthesized Fe-MOF with good peroxidase-like activity could effectively amplify the response signal. Moreover, the prepared aptasensor was able to generate dual-signals of absorbance and current. The outcomes could be mutually verified, providing a high reliability.

The sensitivity of aptasensor is mainly affected by the substrate material, sensing strategy and signal probe. To achieve lower LOD and higher sensitivity, some further works will be tried in the future. (1) Nanomaterial with high large specific surface is used as the substrate material of aptasensor. It helps to fix more aptamer molecules at the sensing interface (Suni, 2021). (2) The strategy of exonuclease-assisted target recycling is applied to the aptasensor for signal intensification (Cao, Xu, Xia, Zhang, & Wang, 2018). (3) Nanoenzyme with higher catalytic activity is employed to prepare the signal probe of the aptasensor (X. Zhu, Chen, Che, & Yan, 2024).

The selectivity of the prepared aptasensor was evaluated using common organophosphorus pesticides, including chlorpyrifos, methyl-parathion, demeton, phoxim and malathion. The response signals of absorbance and current for 100 ng/mL of these organophosphorus pesticides were shown in Fig. 5 e-f. Compared with blank sample, there was no significant change in the signals of absorbance and current in the analysis of chlorpyrifos, methyl-parathion, demeton and phoxim. The signals of absorbance were reduced in the analysis of malathion. Because Fe-MOF was released from the sensing interface in presence of malathion. The results suggested that the prepared aptasensor had a high specificity for malathion. It was attributed to the specific recognition of Apt molecule for malathion. Besides, the relative standard deviation (RSD) was lower than 5 % for both absorbance and current signals, indicating a good repeatability. It was probably because the non-specific

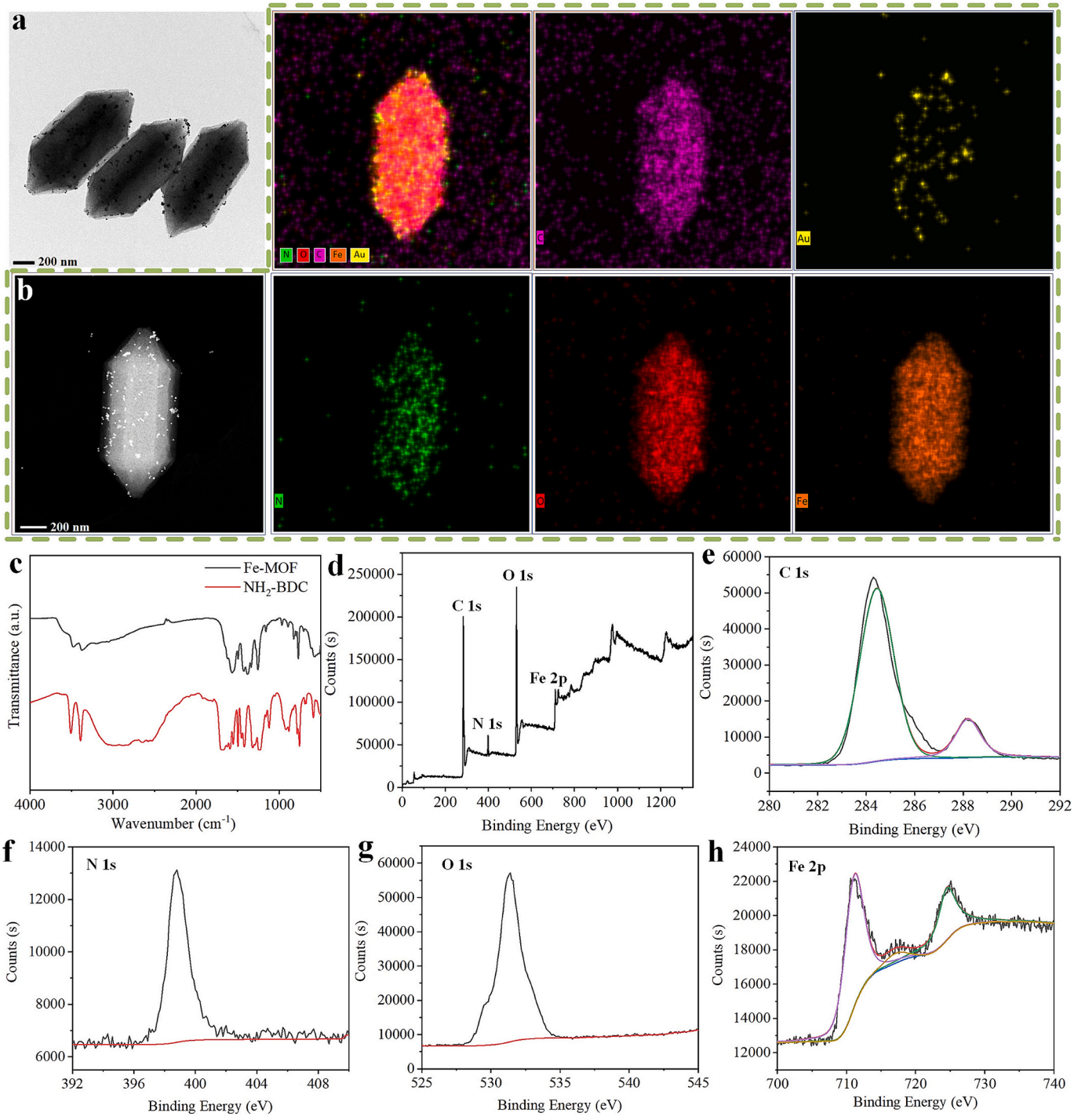

Fig. 2. (a) TEM image of Fe-MOF/AuNPs, (b) EDS mapping images of Fe-MOF/AuNPs for C, N, O, Fe and Au elements, (c) FTIR spectra of Fe-MOF and NH_2-BDC, (d-h) XPS spectra of Fe-MOF.

active sites on sensing interface were effectively blocked by BSA, ensuring a good consistency of the aptasensor.

To investigate the stability, the prepared aptasensors were stored at 4 °C in a refrigerator. During the storage, the aptasensors were daily employed to detect 100 ng/mL malathion. As shown in Fig. S1, the absorbance signal of the aptasensor was 95.30 % of the original absorbance signal, and the current signal of the aptasensor was 95.45 % of the original current signal on the 6th day of storage. The prepared aptasensors could maintained above 95 % of the initial signal intensity after storage for 6 days. The stability of the aptasensor was consistent with that of the reported aptasensors (Hu et al., 2024; Liu et al., 2023). It indicated the favorable stability of the aptasensors.

3.6. Detection of malathion in fruit and vegetable samples

In actual sample analysis, the effect of complex matrices posed a challenge to the malathion detection. To investigate the applicability in complex substrates, fruit and vegetable samples were analyzed by the aptasensor (Table 1). In these samples, malathion was found in celery and cowpea samples. And the rate of positive sample was close to that from previous studies (Yu, Liu, Liu, Wang, & Wang, 2016). The concentration of residual malathion was lower than the maximum residue

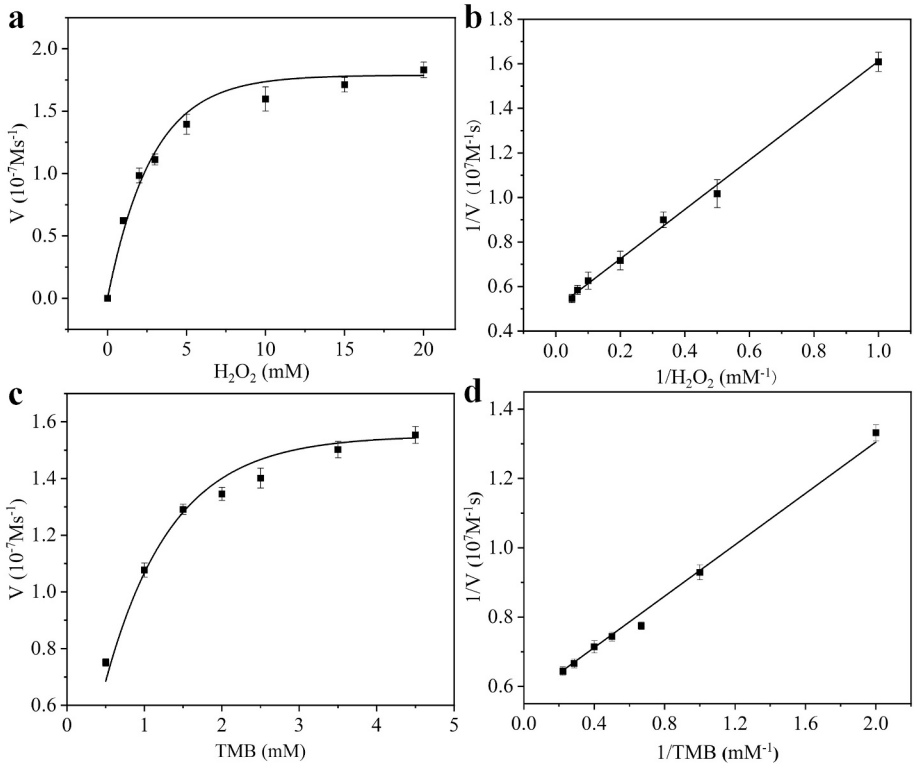

Fig. 3. The Michaelis-Menten curves of Fe-MOF for substrates of (a) H_2O_2 and (c) TMB, the double reciprocal plots for substrates of (b) H_2O_2 and (d) TMB.

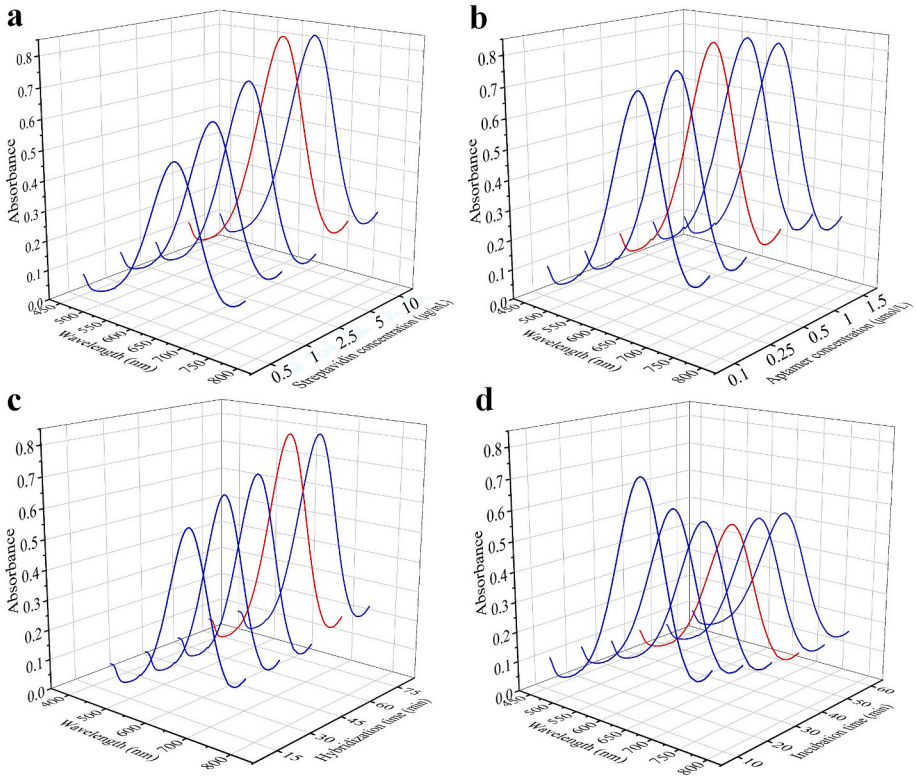

Fig. 4. Effects of (a) streptavidin concentration, (b) Apt concentration, (c) the hybridization time between Apt and cDNA, (d) the incubation time for malathion on the absorbance signal.

limits of national food safety standards in the People's Republic of China (1 mg/kg in celery, 2 mg/kg in cowpea). At the international levels, many studies also showed contamination of malathion in celery and cowpea (Akoto, Andoh, Darko, Eshun, & Osei-Fosu, 2013; Narenderan, Meyyanathan, Karri, Babu, & Chintamaneni, 2019). The recoveries were in the range of 91.48 %%-106.38 % for absorbance signal and 92.94 %–

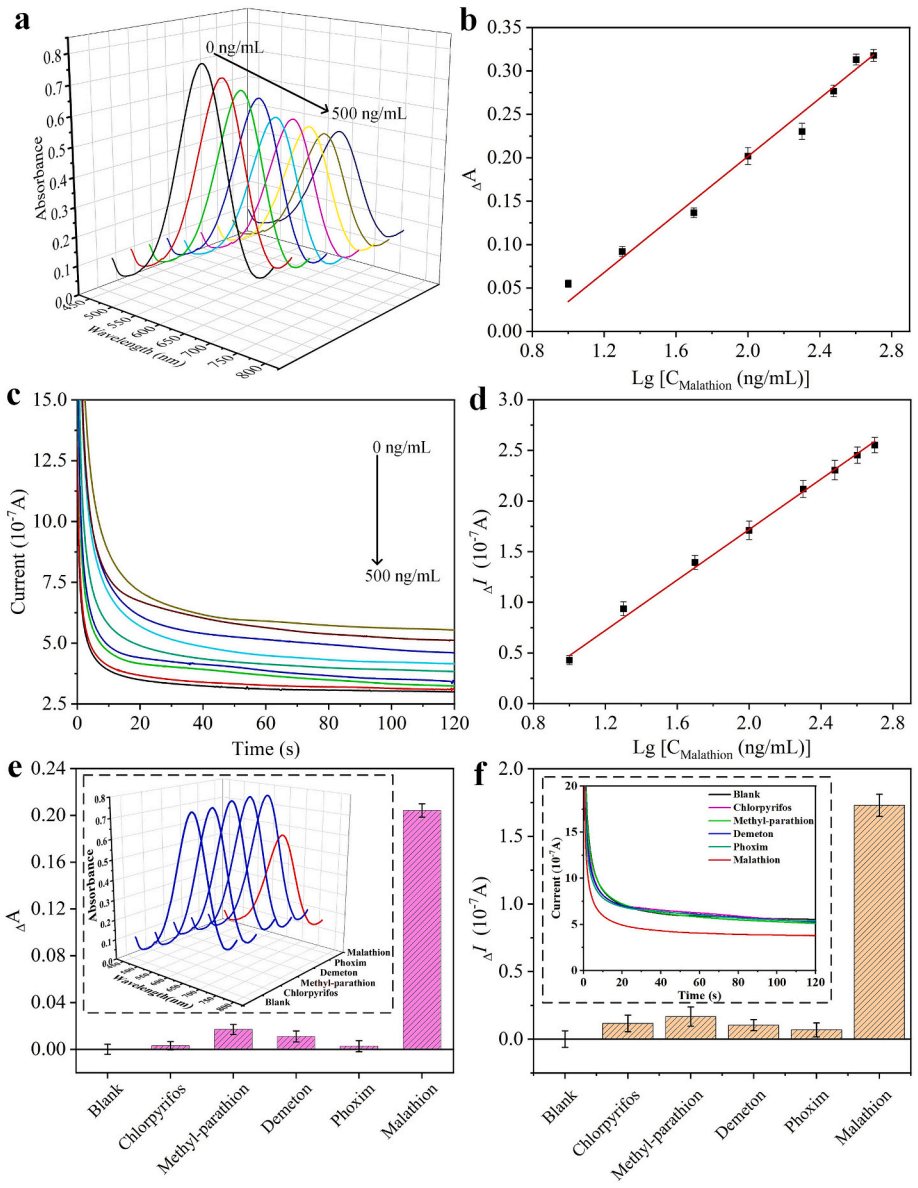

Fig. 5. (a) The UV–Vis spectra for different concentrations of malathion and (b) the corresponding calibration curve, (c) the amperometric i-t curves for different concentrations of malathion and (d) the corresponding calibration curve, the response signals of (e) absorbance and (f) current for organophosphorus pesticides.

107.42 % for current signal. In addition, these samples were analyzed by gas chromatography to validate the accuracy of this method. The outcomes from the aptasensor were in good agreement with those from gas chromatography. These results indicated that the prepared dual-outputs aptasensor had good applicability and accuracy in food samples.

4. Conclusions

An aptasensor with colorimetric and electrochemical dual-outputs was developed for malathion detection. Fe-MOF was synthesized by solvothermal method and verified with excellent peroxidase-like activity by enzymatic kinetics. As a key catalyst, Fe-MOF could catalyze TMB oxidation into oxTMB, producing amplified dual-signals of absorbance and current. Aptamer was able to specificity recognize malathion, and then triggerred the release of Fe-MOF, leading to the reduced dual-signals. Under the optimum conditions, the prepared aptasnesor exhibited sensitive responses for malathion. The detection range of the aptasensor was 10–500 ng/mL of malathion. The LOD of malathion was 5.8 ng/mL for colorimetric output and 4.6 ng/mL for electrochemical output. Besides, the aptasensor had good selectivity and repeatability in malathion detection. Moreover, the prepared aptasensor was successfully applied to detect malathion in fruit and vegetable samples. With these merits, the prepared aptasensor with dual-signals was considered as a powerful rival against the traditional sensors with single-signal in malathion detection.

CRediT authorship contribution statement

Xu Yiwei: Writing – original draft, Funding acquisition, Conceptualization. **Jia Xupeng:** Formal analysis, Data curation. **Yang Sennan:** Software, Methodology. **Cao Mengrui:** Visualization, Validation. **He Baoshan:** Supervision, Project administration. **Ren Wenjie:** Resources. **Suo Zhiguang:** Writing – review & editing.

Declaration of competing interest

The authors declare that they have no known competing financial interests or personal relationships that could have appeared to influence

Table 1
Determination of malathion in fruit and vegetable samples by the dual-outputs aptasensor and gas chromatography ($n = 3$).

Sample	Added (ng/g)	Colorimetric method		Electrochemical method		Gas chromatography
		Found (ng/g)	Recovery	Found (ng/g)	Recovery	Found (ng/g)
Apple	0	0	None	0	None	0
	50	52.45 ± 2.52	104.90 %	48.08 ± 2.04	96.16 %	47.96 ± 1.06
	200	210.57 ± 9.85	105.29 %	205.41 ± 9.27	102.71 %	207.2 ± 5.27
Cabbage	0	0	None	0	None	0
	50	51.84 ± 2.95	103.68 %	46.47 ± 2.53	92.94 %	49.13 ± 1.19
	200	208.16 ± 8.04	104.08 %	206.83 ± 9.34	103.42 %	203.32 ± 6.11
Carrot	0	0	None	0	None	0
	50	46.41 ± 2.03	92.82 %	47.34 ± 2.36	94.68 %	48.12 ± 1.24
	200	189.53 ± 9.65	94.77 %	196.9 ± 8.45	98.45 %	194.11 ± 5.83
Celery	0	139.05 ± 6.69	None	135.32 ± 7.66	None	140.69 ± 2.94
	50	195.51 ± 8.75	103.42 %	191.24 ± 8.56	103.19 %	192.5 ± 6.73
	200	311.46 ± 13.70	91.86 %	315.8 ± 12.97	94.18 %	318.51 ± 8.51
Cowpea	0	64.86 ± 3.43	None	61.21 ± 2.65	None	65.42 ± 1.28
	50	118.27 ± 5.19	102.97 %	116.93 ± 5.46	105.14 %	115.81 ± 4.03
	200	251.29 ± 11.45	94.88 %	256.59 ± 10.82	98.23 %	261.14 ± 9.31
Eggplant	0	0	None	0	None	0
	50	45.74 ± 2.18	91.48 %	47.29 ± 1.90	94.58 %	48.59 ± 1.36
	200	191.87 ± 8.59	95.94 %	194.25 ± 8.91	97.13 %	197.02 ± 5.76
Green pepper	0	0	None	0	None	0
	50	46.55 ± 2.27	93.10 %	48.31 ± 2.15	96.62 %	49.04 ± 1.64
	200	201.29 ± 8.06	100.65 %	204.64 ± 9.23	102.32 %	207.95 ± 6.82
Pear	0	0	None	0	None	0
	50	52.13 ± 1.86	104.26 %	53.71 ± 2.58	107.42 %	51.32 ± 1.27
	200	187.48 ± 7.94	93.74 %	192.14 ± 8.60	96.07 %	194.36 ± 5.80
Spinach	0	0	None	0	None	0
	50	47.71 ± 1.93	95.42 %	49.16 ± 2.25	98.32 %	50.73 ± 1.57
	200	197.18 ± 8.59	98.59 %	204.33 ± 10.16	102.17 %	206.42 ± 4.72
Tomato	0	0	None	0	None	0
	50	53.19 ± 2.56	106.38 %	52.08 ± 2.64	104.16 %	51.16 ± 1.06
	200	207.47 ± 7.35	103.74 %	213.52 ± 9.67	106.76 %	204.29 ± 4.15

the work reported in this paper.

Data availability

Data will be made available on request.

Acknowledgements

The authors gratefully acknowledge the financial support provided by the Open Project of National Engineering Laboratory for Deep Processing of Wheat, Corn (NL2022019), the Project of Research and Development of Zhengzhou (22ZZRDZX24), the Natural Science Foundation of Henan University of Technology (2022BS022), the Natural Science Foundation of Henan Province (242300421559).

Appendix A. Supplementary data

Supplementary data to this article can be found online at https://doi.org/10.1016/j.fochx.2024.101835.

References

Abdo, W., Elmadawy, M. A., Abdelhiee, E. Y., Abdel-Kareem, M. A., Farag, A., Aboubakr, M., … Fadl, S. E. (2021). Protective effect of thymoquinone against lung intoxication induced by malathion inhalation. *Scientific Reports, 11*(1), 2498. https://doi.org/10.1038/s41598-021-82083-w

Akoto, O., Andoh, H., Darko, G., Eshun, K., & Osei-Fosu, P. (2013). Health risk assessment of pesticides residue in maize and cowpea from Ejura. *Ghana. Chemosphere, 92*(1), 67–73. https://doi.org/10.1016/j.chemosphere.2013.02.057

Bala, R., Mittal, S., Sharma, R. K., & Wangoo, N. (2018). A supersensitive silver nanoprobe based aptasensor for low cost detection of malathion residues in water and food samples. *Spectrochimica Acta Part A: Molecular and Biomolecular Spectroscopy, 196*, 268–273. https://doi.org/10.1016/j.saa.2018.02.007

Bala, R., Swami, A., Tabujew, I., Peneva, K., Wangoo, N., & Sharma, R. K. (2018). Ultrasensitive detection of malathion using quantum dots-polymer based fluorescence aptasensor. *Biosensors and Bioelectronics, 104*, 45–49. https://doi.org/10.1016/j.bios.2017.12.034

Bazmandegan-Shamili, A., Haji Shabani, A. M., Dadfarnia, S., Rohani Moghadam, M., & Saeidi, M. (2017). Preparation of magnetic mesoporous silica composite for the solid-phase microextraction of diazinon and malathion before their determination by high-performance liquid chromatography. *Journal of Separation Science, 40*(8), 1731–1738. https://doi.org/10.1002/jssc.201601339

Cao, X., Xu, J., Xia, J., Zhang, F., & Wang, Z. (2018). An electrochemical aptasensor based on the conversion of liquid-phase colorimetric assay into electrochemical analysis for sensitive detection of lysozyme. *Sensors and Actuators B: Chemical, 255*, 2136–2142. https://doi.org/10.1016/j.snb.2017.09.019

Chen, Q., Sheng, R., Wang, P., Ouyang, Q., Wang, A., Ali, S., … Hassan, M. M. (2020). Ultra-sensitive detection of malathion residues using FRET-based upconversion fluorescence sensor in food. *Spectrochimica Acta Part A: Molecular and Biomolecular Spectroscopy, 241*, Article 118654. https://doi.org/10.1016/j.saa.2020.118654

Chen, Y., Meng, X.-Z., Gu, H.-W., Yi, H.-C., & Sun, W.-Y. (2019). A dual-response biosensor for electrochemical and glucometer detection of DNA methyltransferase activity based on functionalized metal-organic framework amplification. *Biosensors and Bioelectronics, 134*, 117–122. https://doi.org/10.1016/j.bios.2019.03.051

Davydova, A. S., & Vorobyeva, M. A. (2024). Aptasensors based on non-enzymatic peroxidase mimics: Current Progress and challenges. *Biosensors, 14*(1), 1. https://doi.org/10.3390/bios14010001

Faghiri, F., Hajjami, M., & Ghorbani, F. (2021). Development of a sensing system based on coupling magnetic solid phase extraction and colorimetric detection for determination of organophosphorus pesticides in fruit extract and environmental sample. *Sensors and Actuators B: Chemical, 343*, Article 130157. https://doi.org/10.1016/j.snb.2021.130157

Gao, L., Zhuang, J., Nie, L., Zhang, J., Zhang, Y., Gu, N., Wang, T., Feng, J., Yang, D., Perrett, S., & Yan, X. (2007). Intrinsic peroxidase-like activity of ferromagnetic nanoparticles. *Nature Nanotechnology, 2*(9), 577–583. https://doi.org/10.1038/nnano.2007.260

Gupta, N., Singh, R., Nayak, S. K., Das, M., & Jan, K. (2022). Development and validation of multiresidue method for organophosphorus pesticides in lanolin using gas chromatography–tandem mass spectrometry. *Journal of Mass Spectrometry, 57*(11), Article e4894. https://doi.org/10.1002/jms.4894

Hu, M., Dong, J., Wang, H., Huang, J., Geng, L., Liu, M., … Guo, Y. (2024). Novel ratiometric electrochemical aptasensor based on broad-spectrum aptamer recognition for simultaneous detection of penicillin antibiotics in milk. *Food Chemistry, 456*, Article 139946. https://doi.org/10.1016/j.foodchem.2024.139946

Hu, W.-C., Younis, M. R., Zhou, Y., Wang, C., & Xia, X.-H. (2020). In situ fabrication of Ultrasmall gold nanoparticles/2D MOFs hybrid as Nanozyme for antibacterial therapy. *Small, 16*(23), 2000553. https://doi.org/10.1002/smll.202000553

Li, P., Zhan, H. N., Tao, S. J., Xie, Z. H., & Huang, J. H. (2023). Bio-inspired aptamers decorated gold nanoparticles enable visualized detection of malathion. *Frontiers in Bioengineering and Biotechnology, 11*. https://doi.org/10.3389/fbioe.2023.1165724

Li, W., Chen, J., Linli, F., Chen, X., Huang, Y., & Yang, X. (2023). Organophosphorus pesticide contaminants in fruits and vegetables: A meta-analysis. *Food Chemistry: X, 20*, Article 101014. https://doi.org/10.1016/j.fochx.2023.101014

Li, Y., Javed, R., Li, R., Zhang, Y., Lang, Z., Zhao, H., Liu, X., Cao, H., & Ye, D. (2023). A colorimetric smartphone-based sensor for on-site AA detection in tropical fruits using Fe-P/NC single-atom nanoenzyme. *Food Chemistry, 406*, Article 135017. https://doi.org/10.1016/j.foodchem.2022.135017

Li, Y., Jiang, J., Fang, Y., Cao, Z., Chen, D., Li, N., Xu, Q., & Lu, J. (2018). TiO2 Nanoparticles Anchored onto the Metal–Organic Framework NH2-MIL-88B(Fe) as an Adsorptive Photocatalyst with Enhanced Fenton-like Degradation of Organic Pollutants under Visible Light Irradiation. *ACS Sustainable Chemistry & Engineering, 6*(12), 16186–16197. https://doi.org/10.1021/acssuschemeng.8b02968

Liang, N., Hu, X., Li, W., Mwakosya, A. W., Guo, Z., Xu, Y., … Shi, J. (2021). Fluorescence and colorimetric dual-mode sensor for visual detection of malathion in cabbage based on carbon quantum dots and gold nanoparticles. *Food Chemistry, 343*, Article 128494. https://doi.org/10.1016/j.foodchem.2020.128494

Liu, P., Li, X., Xu, X., Niu, X., Wang, M., Zhu, H., & Pan, J. (2021). Analyte-triggered oxidase-mimetic activity loss of Ag3PO4/UiO-66 enables colorimetric detection of malathion completely free from bioenzymes. *Sensors and Actuators B: Chemical, 338*, Article 129866. https://doi.org/10.1016/j.snb.2021.129866

Liu, S., Meng, S., Wang, M., Li, W., Dong, N., Liu, D., Li, Y., & You, T. (2023). In-depth interpretation of aptamer-based sensing on electrode: Dual-mode electrochemical-photoelectrochemical sensor for the ratiometric detection of patulin. *Food Chemistry, 410*, Article 135450. https://doi.org/10.1016/j.foodchem.2023.135450

Narenderan, S. T., Meyyanathan, S. N., Karri, V. V. S. R., Babu, B., & Chintamaneni, P. (2019). Multivariate response surface methodology assisted modified QuEChERS extraction method for the evaluation of organophosphate pesticides in fruits and vegetables cultivated in Nilgiris. *South India. Food Chemistry, 300*, Article 125188. https://doi.org/10.1016/j.foodchem.2019.125188

Nie, Y., Teng, Y., Li, P., Liu, W., Shi, Q., & Zhang, Y. (2018). Label-free aptamer-based sensor for specific detection of malathion residues by surface-enhanced Raman scattering. *Spectrochimica Acta Part A: Molecular and Biomolecular Spectroscopy, 191*, 271–276. https://doi.org/10.1016/j.saa.2017.10.030

Pupim, A. C. E., Basso, C. R., Machado, C. C. A., Watanabe, P. S., Fernandes, G. S. A., ErthalL, R. P., … Araújo, E. J. A. (2023). Long-term and low dose oral malathion exposure causes morphophysiological changes in the colon of rats. *Life Sciences, 327*, Article 121840. https://doi.org/10.1016/j.lfs.2023.121840

Rizk, M. A., Alsaiari, M. A., Alsaiari, R. A., Ibrahim, I. A., Abbas, A. M., & Khairy, G. M. (2023). New terbium complex as a luminescent sensor for the highly selective detection of malathion in water samples. *Chemosensors, 11*(12), 570. https://doi.org/10.3390/chemosensors11120570

Serebrennikova, K. V., Komova, N. S., Aybush, A. V., Zherdev, A. V., & Dzantiev, B. B. (2023). Flexible substrate of cellulose Fiber/structured Plasmonic silver nanoparticles applied for label-free SERS detection of malathion. *Materials, 16*(4), 1475. https://doi.org/10.3390/ma16041475

Shu, R., Liu, S., Huang, L., Li, Y., Sun, J., Zhang, D., Zhu, M.-Q., & Wang, J. (2022). Enzyme-mimetic nano-immunosensors for amplified detection of food hazards: Recent advances and future trends. *Biosensors and Bioelectronics, 217*, Article 114577. https://doi.org/10.1016/j.bios.2022.114577

Suni, I. I. (2021). Substrate materials for biomolecular immobilization within electrochemical biosensors. *Biosensors, 11*(7), 239. https://doi.org/10.3390/bios11070239

Thajee, K., Paengnakorn, P., Wongwilai, W., & Grudpan, K. (2018). Application of a webcam camera as a cost-effective sensor with image processing for dual electrochemical – Colorimetric detection system. *Talanta, 185*, 160–165. https://doi.org/10.1016/j.talanta.2018.03.055

Wang, X., Dong, S., & Wei, H. (2023). Recent advances on Nanozyme-based electrochemical biosensors. *Electroanalysis, 35*(1), Article e202100684. https://doi.org/10.1002/elan.202100684

Warkhade, S. K., Singh, R. P., Das, R. S., Gaikwad, G. S., Zodape, S. P., Pratap, U. R., … Wankhade, A. V. (2021). CoSe2 nanoflakes: An artificial nanoenzyme with excellent peroxidase like activity. *Inorganic Chemistry Communications, 126*, Article 108461. https://doi.org/10.1016/j.inoche.2021.108461

Williams, M. R., Maher, E., & Sooter, J. L. (2014). In vitro selection of a single-stranded DNA molecular recognition element for the pesticide malathion. *Combinatorial Chemistry & High Throughput Screening, 17*(8), 694–702. https://doi.org/10.2174/1386207317666140827123631

Xie, F.-T., Zhao, X.-L., Chi, K.-N., Yang, T., Hu, R., & Yang, Y.-H. (2020). Fe-MOFs as signal probes coupling with DNA tetrahedral nanostructures for construction of ratiometric electrochemical aptasensor. *Analytica Chimica Acta, 1135*, 123–131. https://doi.org/10.1016/j.aca.2020.08.007

Xu, G., Huo, D., Hou, J., Zhang, C., Zhao, Y., Hou, C., Bao, J., Yao, X., & Yang, M. (2021). An electrochemical aptasensor of malathion based on ferrocene/DNA-hybridized MOF, DNA coupling-gold nanoparticles and competitive DNA strand reaction. *Microchemical Journal, 162*, Article 105829. https://doi.org/10.1016/j.microc.2020.105829

Yılmaz, F., Ünlüer, Ö. B., Ersöz, A., & Say, R. (2018). Multifunctional nanoenzymes from carbonic anhydrase skeleton. *Process Biochemistry, 72*, 71–78. https://doi.org/10.1016/j.procbio.2018.06.005

Yiwei, X., Yahui, L., Weilong, T., Jiyong, S., Xiaobo, Z., Wen, Z., Xinai, Z., Yanxiao, L., Changqiang, Z., Lele, A., Hong, L., & Tingting, S. (2021). Electrochemical determination of hantavirus using gold nanoparticle-modified graphene as an electrode material and cu-based metal-organic framework assisted signal generation. *Microchimica Acta, 188*(4), 112. https://doi.org/10.1007/s00604-021-04769-2

Yu, R., Liu, Q., Liu, J., Wang, Q., & Wang, Y. (2016). Concentrations of organophosphorus pesticides in fresh vegetables and related human health risk assessment in Changchun, Northeast China. *Food Control, 60*, 353–360. https://doi.org/10.1016/j.foodcont.2015.08.013

Zhan, Y., Xie, F., Zhang, H., Jin, Y., Meng, H., Chen, J., & Sun, X. (2020). Highly dispersed nonprecious metal catalyst for oxygen reduction reaction in proton exchange membrane fuel cells. *ACS Applied Materials & Interfaces, 12*(15), 17481–17491. https://doi.org/10.1021/acsami.0c00126

Zhang, X., Li, G., Wu, D., Li, X., Hu, N., Chen, J., Chen, G., & Wu, Y. (2019). Recent progress in the design fabrication of metal-organic frameworks-based nanozymes and their applications to sensing and cancer therapy. *Biosensors and Bioelectronics, 137*, 178–198. https://doi.org/10.1016/j.bios.2019.04.061

Zhu, C., Wang, X., Yu, D., Chen, L., & Han, X. (2023). Hairpin DNA-enabled ratiometric electrochemical aptasensor for detection of malathion. *Microchimica Acta, 190*(5), 167. https://doi.org/10.1007/s00604-023-05760-9

Zhu, X., Chen, C., Che, D., & Yan, H. (2024). A high oxidase-like activity, bimetallic single-atom nanozyme FeCe/NC prepared by FeCe-ZIF-8 approach for sensing tannic acid in tea. *Food Chemistry: X, 23*, Article 101552. https://doi.org/10.1016/j.fochx.2024.101552